Rare Metal Materials and Engineering
Volume 55, Issue 4, April 2026
Available online at www.rmme.ac.cn

Science Press

Cite this article as: Gao Huixian, Li Ke, Shao Shan, et al. Orthogonal Optimization of Solution Treatment and Aging Process for TB18 Titanium Alloy and Toughness Regulation Mechanism[J]. Rare Metal Materials and Engineering, 2026, 55(04): 841-855. DOI: https://doi.org/10.12442/j.issn.1002-185X.20250284.

ARTICLE

Orthogonal Optimization of Solution Treatment and Aging Process for TB18 Titanium Alloy and Toughness Regulation Mechanism

Gao Huixian[1,2], Li Ke[2], Shao Shan[2], Yang Haoxue[1], Li Qinqin[1,2], Zhao Yanru[2], Luo Wenzhong[1,2], Feng Yong[1,2], Lei Qiang[1,2], Liu Xianghong[1,2]

[1] School of Materials Science and Engineering, Northwestern Polytechnical University, Xi'an 710072, China; [2] Western Superconducting Technologies Co., Ltd, Xi'an 710018, China

Abstract: To investigate the effect of solution treatment and aging process parameters on the microstructure and mechanical properties of TB18 titanium alloy, process optimization research was conducted based on the mixed-level orthogonal experiment design of factor levels. Results show that through range analysis, the significance order of process parameters is determined as follows: solution cooling method>solution temperature>aging time>aging temperature>solution time. Considering the strength-ductility matching and engineering application requirements, the benchmark parameters are selected as solution time of 1 h, solution cooling method of air cooling (AC), aging temperature of 525 °C, and aging time of 4 h. Furthermore, the effects of solution temperature in the range of 790−870 °C on the impact toughness and micro-fracture characteristics of the alloy were studied. The results reveal that the larger the area of shear lip and fibrous zone, and the smaller the area of radiation zone, the better the toughness of the alloy. With the increase in solution temperature, the length of secondary cracks on the fracture surface increases, the number of dimples increases, and the toughness is enhanced. Based on the collaborative optimization of strength and toughness, the optimal heat treatment process for TB18 alloy is determined as 870 °C/1 h, AC+525 °C/4 h, AC.

Key words: TB18 titanium alloy; solution and aging; orthogonal test; toughness; microstructure

1 Introduction

Against the backdrop of the continuous pursuit of high-performance materials in aerospace and other high-end fields, titanium alloys have become the unrivaled choice for key structural materials due to their high specific strength, excellent corrosion resistance, and superior high-temperature performance. Among them, metastable β-type titanium alloys have attracted considerable attention because of their unique phase transformation behavior and microstructure evolution mechanisms, which endow them with exceptional comprehensive mechanical properties[1–2].

Solution and aging treatment are usually the core methods to improve the mechanical properties of metastable β titanium alloys[3–4]. By heating the β titanium alloy to a specific temperature range, the full dissolution of alloying elements into the β phase is accelerative, forming a supersaturated solid solution and laying the foundation for precipitation during subsequent aging. Then, the aging is adopted to precisely control the type, size, morphology, and distribution of precipitates in the supersaturated solid solution by manipulating temperature and time, thereby achieving the expected mechanical properties[5–7]. To obtain fine grain structure, a solution treatment was conducted on the hot-rolled Ti-Al-Mo-V-Cr-Nb alloys, followed by aging at 525 °C[8]. The results showed that the $\alpha+\beta$ rolled alloy exhibits a tensile strength of 1550 MPa and ductility of 6.5% after aging, with α/β interface strengthening as the main strengthening mode. Uniformly distributed fine β grains and microscale primary α phases facilitate better coordination of deformation, thereby improving ductility. Naydenkin et al[9] investigated the effects of aging treatment on the microstructure and mechanical

Received date: May 23, 2025
Foundation item: Key Program of National Natural Science Foundation of China (52431001)
Corresponding author: Liu Xianghong, Ph. D., Professor, Western Superconducting Technology Co., Ltd, Xi'an 710018, P. R. China, E-mail: 15754303726@163.com

properties of Ti-15V-3Cr-3Al-3Sn-1Zr-1Mo alloy produced by rotary swaging. It was found that the tensile strength is increased from 800 MPa to 1550 MPa while maintaining ductility of approximately 4% after aging at 420 °C for 10 h. When the aging temperature increases to 450 °C, the strength is decreased due to the aggregation of lamellar α/α'' phase and reduced internal stress in the β phase.

The combination of thermomechanical processing and heat treatment effectively regulates the microstructure of the β titanium alloys, thereby enhancing the mechanical properties[10–11]. However, heat treatment processes are often complicated by the interactive effects of multiple factors, such as heating temperature, holding time, and cooling method. Moreover, due to the inconsistent number of values across multiple factors, an in-depth understanding of the quantitative relationships between process parameters and microstructural evolution remains lacking, making it difficult to accurately predict and adjust the mechanical properties of β titanium alloys[12–14]. Besides, the large-sized as-forged β titanium alloys exhibit non-uniform distribution of the temperature between the surface and core during aging due to size effect, leading to microstructural and property discrepancies, and thus severely affecting material reliability and safety in service[15]. Additionally, the stability of toughness and the synergistic optimization mechanism among strength, plasticity, and toughness under complex service environments still require further clarification[16–17].

Distinct from conventional $\alpha+\beta$ titanium alloys that tend to develop property gradients in large-scale components, the newly developed metastable β titanium alloy, TB18, characterized by a high content of β-stabilizing elements, is capable of maintaining uniform distribution of mechanical properties in thick-section parts. As a precipitation-strengthened alloy, the mechanical properties of TB18 alloy largely depend on the size, morphology, and volume fraction of the α precipitated phase during aging[18]. After solution treatment, the alloy presents an equiaxed β-grain microstructure, while during aging, secondary α phase precipitates uniformly in a lamellar configuration within the β matrix. The size uniformity of these precipitates exerts a critical influence on achieving the optimal strength-toughness balance. Contrary to the dispersion strengthening mechanism of α phases in traditional titanium alloys, the precipitation strengthening effect in TB18 stems from fine α lamellae precipitated within the β matrix. This unique strengthening mechanism enables the alloy to retain superior fatigue resistance even at a high strength level of 1300 MPa. Despite the fact that TB18 titanium alloy possesses superior overall performance with both high strength and high toughness in the β-annealed state, its plasticity modulation remains challenging due to a relatively low initial plasticity level. In metastable β titanium alloys, retaining a small amount of equiaxed primary α phase (α_p) can effectively inhibit the occurrence of the β embrittlement phenomenon while maintaining good plasticity. Therefore, implementing solution and aging treatment for the TB18 titanium alloy, constructing diverse microstructures through the precise control of aging temperature, combining mechanical property testing and microstructural characterization, and deeply exploring the action mechanism of process parameters on microstructural evolution and plasticity regulation are important research directions for achieving the synergistic optimization of strength, toughness, and plasticity.

The solution and aging treatment of TB18 titanium alloy involves multiple key parameters such as solution temperature, solution time, solution cooling method, aging temperature, and aging time, with significant differences in the number of levels among these parameters. The influence of parameter variation on the microstructure and mechanical properties is complex. If the single-factor test method is adopted, it not only fails to reflect the synergistic effects among multiple factors, but also requires full-combination tests, which involves an extremely large number of tests and is inefficient, making it difficult to quickly screen out key influencing factors. However, the mixed orthogonal test method can target multi-factor systems with different numbers of levels. By reasonably designing the orthogonal array, it can significantly reduce the number of tests while effectively analyzing the main effects and interaction effects of each factor, which is particularly suitable for optimizing the process of alloys like TB18 that are affected by multiple parameters. Based on this conclusion, this study first optimized the solution and aging process of TB18 alloy through the mixed orthogonal test. On the one hand, it efficiently determined the significance order of the influence of each parameter on strength and plasticity, and screened out the benchmark process with excellent comprehensive strength and plasticity. On the other hand, based on the orthogonal optimization results, it focused on key parameters and conducted in-depth research on their influence laws on impact toughness, thereby revealing the toughness regulation mechanism and influencing factors under different conditions.

2 Experiment

2.1 Orthogonal experiment design of solution and aging treatment

Vacuum consumable melting was adopted to prepare the β-type TB18 titanium alloy with a nominal composition of Ti-4Al-5Mo-5V-5Cr-1Nb. The ingot was remelted three times to ensure uniform composition and impurity removal, and then it was processed into a bar of Φ400 mm through multiple forging operations in the β region and $\alpha+\beta$ dual-phase region.

Five test parameters were selected: solution temperature (A), solution holding time (B), solution cooling mode (C), aging temperature (D), and aging time (E). Among them, solution temperature (A), a critical parameter for β-type titanium alloys, directly governs the dissolution extent of the β phase and grain size. Solution holding time (B) affects the homogenization level of alloying elements within the β phase, that is, sufficient holding duration ensures complete dissolution of alloying elements and mitigates compositional segregation, while excessively prolonged duration may induce

coarsening of β grains. Different solution cooling modes (C) influence the retention degree of the β phase through variations in cooling rates, thereby modulating the nucleation driving force of the α phase during aging. Aging temperature (D) and aging time (E) collectively decide the size, morphology, and distribution of α precipitates. Aging temperature directly influences atomic diffusion kinetics, while aging time dictates the volume fraction of precipitates. Insufficient precipitation may occur with short aging duration whereas excessive duration can lead to coarsening. Therefore, they are core parameters for tailoring the strength-plasticity balance. Furthermore, based on existing studies[19–21] and preliminary experiments, this study incorporated varying numbers of levels for each parameter. The selection of solution temperature was primarily rooted in the phase transformation characteristics of TB18 titanium alloy, specifically the $\alpha+\beta$ dual-phase region and β single-phase region. Prior research has demonstrated that aging near 525 °C facilitates the precipitation of secondary α phases with a more uniform distribution. Therefore, a narrow range of aging temperatures is initially adopted, which will be extended to 450–575 °C in subsequent experiments to validate the impact of aging temperature on morphology of α phase and toughness of alloy. Specifically, A had 6 levels, B had 3 levels, C had 3 levels, D had 4 levels, and E had 3 levels. The mixed orthogonal test factors and levels are shown in Table 1. The orthogonal test scheme is presented in Table 2, with a total of 25 heat treatment tests conducted. Then, the samples were subjected to solution and aging treatment via a box resistance furnace. They were heated to the set temperature and held for the corresponding time, followed by cooling according to specified cooling mode.

2.2 Characterization method

The samples with a size of 10 mm×10 mm×15 mm were subjected to rough grinding, fine grinding, rough polishing, and fine polishing, followed by etching with Kroll's reagent (5 mL HF+13 mL HNO_3+82 mL H_2O). The microstructure was observed using a ZEISS optical microscope (OM) and a JEOL IT700 field emission scanning electron microscope (SEM). For tensile property testing, three samples were taken for each test. After heat treatment, samples were machined into standard rod-shaped tensile samples with a gauge length of 25 mm and a diameter of 5 mm. The length and direction of the tensile samples were parallel to the axis of the sample piece. Room-temperature tensile tests were performed on a Zwick/Roell Z100 universal tensile testing machine at a tensile rate of 0.25 mm/s. The average values of tensile strength, yield strength, elongation after fracture, and reduction of area from the three samples in each test group were calculated as the results.

2.3 Impact test

The oscilloscopic impact test was conducted using an MHLC-7000WY (oscilloscopic) drop-weight impact testing machine. The impact blank samples with a size of 10 mm× 10 mm×55 mm were subjected to heat treatment with solution temperatures of 790, 810, 840, and 870 °C for 1 h, followed by air cooling (AC) and aging at 525 °C for 2 h. For the samples solution treated at 870 °C, aging was performed at 450, 490, 525, and 575 °C for 4 h, followed by AC, separately. After heat treatment, oscilloscopic impact tests were conducted. The impact fracture morphology was observed using SEM to analyze the fracture characteristics.

3 Results and Discussion

3.1 Analysis of mixed-level orthogonal experiment result

Tensile strength R_m, yield strength $R_{p0.2}$, elongation after fracture A, and reduction of area Z were chosen as the test indices for this experiment. The experimental results are presented in Table 3, with the calculations given in Eq. (1–4).

$$k_{j,l} = \sum y_{j,l,i} \tag{1}$$

$$\bar{k}_{j,l} = \frac{k_{j,l}}{r} \tag{2}$$

$$r = \frac{n}{m} \tag{3}$$

$$R_j = \max\left(\bar{k}_{j,1},\bar{k}_{j,2},\bar{k}_{j,3},\cdots,k_{j,m}\right) - \min\left(\bar{k}_{j,1},\bar{k}_{j,2},\bar{k}_{j,3},\cdots,k_{j,m}\right) \tag{4}$$

where n is the number of experiments; m is the number of levels of the factor; $y_{j,l,i}$ represents the result of the ith experiment at the lth level of factor j with i=1, 2, ..., n; $k_{j,l}$ denotes the sum of all corresponding experimental results when factor j is at the lth level (l=1, 2, ..., m); $\bar{k}_{j,l}$ is the average result when factor j is at the lth level; r is the number of times each level appears in the experiments; R_j is the range of factor j.

The results of the orthogonal experiment are calculated and analyzed using the range analysis method for orthogonal experiments, and the results are shown in Table 4. The range R

Table 1 Factor level of orthogonal test

Level	Factor				
	Solution temperature, A/°C	Solution time, B/h	Solution cooling method, C	Aging temperature, D/°C	Aging time, E/h
1	760	1	AC	520	2
2	790	2	WQ	525	4
3	810	4	FC	530	6
4	840	-	-	535	-
5	870	-	-	-	-
6	900	-	-	-	-

Note: WQ means water quenching and FC means furnace cooling.

Table 2 Orthogonal test scheme

No.	Solution temperature, A/°C	Solution time, B/h	Solution cooling method, C	Aging temperature, D/°C	Aging time, E/h	Heat treatment
1	760	1	AC	520	2	760 °C/1 h, AC+520 °C/2 h, AC
2	760	1	AC	535	6	760 °C/1 h, AC+535 °C/6 h, AC
3	760	2	WQ	525	4	760 °C/2 h, WQ+525 °C/4 h, AC
4	760	4	FC	530	6	760 °C/4 h, FC+530 °C/6 h, AC
5	790	1	AC	525	6	790 °C/1 h, AC+525 °C/6 h, AC
6	790	1	WQ	530	4	790 °C/1 h, WQ+530 °C/4 h, AC
7	790	2	FC	520	2	790 °C/2 h, FC+520 °C/2 h, AC
8	790	4	WQ	535	2	790 °C/4 h, WQ+535 °C/6 h, AC
9	810	1	FC	530	4	810 °C/1 h, FC+530 °C/4 h, AC
10	810	2	AC	525	2	810 °C/2 h, AC+525 °C/2 h, AC
11	810	2	WQ	535	4	810 °C/2 h, WQ+535 °C/4 h, AC
12	810	4	WQ	520	6	810 °C/4 h, WQ+520 °C/6 h, AC
13	840	1	FC	520	2	840 °C/1 h, FC+520 °C/2 h, AC
14	840	2	AC	530	6	840 °C/2 h, AC+530 °C/6 h, AC
15	840	4	AC	535	4	840 °C/4 h, AC+535 °C/4 h, AC
16	840	4	WQ	525	2	840 °C/4 h, WQ+525 °C/2 h, AC
17	870	1	WQ	530	2	870 °C/1 h, WQ+530 °C/2 h, AC
18	870	1	WQ	535	2	870 °C/1 h, WQ+535 °C/2 h, AC
19	870	2	AC	525	4	870 °C/2 h, AC+525 °C/4 h, AC
20	870	2	FC	535	6	870 °C/2 h, FC+535 °C/6 h, AC
21	870	4	AC	520	4	870 °C/4 h, AC+520 °C/4 h, AC
22	900	1	FC	525	4	900 °C/1 h, FC+525 °C/4 h, AC
23	900	2	WQ	530	2	900 °C/2 h, WQ+530 °C/2 h, AC
24	900	2	AC	535	4	900 °C/2 h, AC+535 °C/4 h, AC
25	900	4	AC	520	6	900 °C/4 h, AC+520 °C/6 h, AC

reflects the magnitude of the influence of each factor on the test indices in the experiment. A larger range indicates that the factor has a greater influence on the test index and is usually a primary factor, while a smaller range indicates a smaller influence and is usually a secondary factor. As can be seen from Table 4, among all indicators, C yields the largest R values except for Z: R_m is 223.0, $R_{p0.2}$ is 234.1, A is 6.8, and Z is 15.6, which is slightly lower than 16.0. Since the cooling rate directly determines the stability of the supersaturated solid solution after solution treatment, it exerts the most direct regulatory effect on the morphology, volume fraction, and distribution of the α phase, and further regulates the strength and plasticity of the alloy, thus having the most significant impact.

According to the calculation results, the primary and secondary influencing factors for the four test indices are ranked in descending order of range as follows: for R_m, C>E>D>A>B; for $R_{p0.2}$, C>E>A>D>B; for A, C>A>E>D>B; for Z, A>C>E>D>B. It can be seen that factor C is the most important factor affecting each index, and the order of influence of the other four factors on the indices is A>E>D>B. For strength, it mainly relies on the strengthening effect of the secondary α (α_s) phase precipitated during aging. The aging time (E) directly affects the volume fraction of α_s. The excessively long time tends to cause coarsening, while the excessively short time leads to insufficient precipitation, which may be the reason why the influence of aging time (E) is greater than that of aging temperature (D). The solution temperature (A) affects the driving force of α_s precipitation by changing the saturation degree of the β phase, but its influence is weaker than that of aging time (E). Plasticity is more related to grain size, α_p phase content, and α_s morphology. The solution temperature (A) determines the content of the α_p phase. Solution treatment in the dual-phase region usually retains more α_p, inhibiting β embrittlement, and thus enhancing the influence of solution temperature (A) on plasticity. The cooling method (C) affects plasticity through the morphology of α_s. For example, the coarse α_s formed by FC can better accommodate deformation, but its influence on Z is weaker than that of solution temperature (A).

Fig. 1 shows the relationships between factors and evaluation indices. It can be seen that the optimal level combinations of each factor for the four indices are as follows: $A_2B_1C_1D_2E_2$ for R_m, $A_2B_1C_1D_2E_2$ for $R_{p0.2}$, $A_2B_3C_3D_3E_1$ for A, and $A_1B_3C_3D_3E_1$ for Z. Among them, the optimal factor level combinations corresponding to R_m and $R_{p0.2}$ are the same,

Table 3 Results of orthogonal test

No.	Factor					Mechanical properties			
	Solution temperature, A/°C	Solution time, B/h	Solution cooling method, C	Aging temperature, D/°C	Aging time, E/h	R_m/MPa	$R_{p0.2}$/MPa	A/%	Z/%
1	760	1	AC	520	2	1398	1334	7.5	20
2	760	1	AC	535	6	1355	1301	9.7	22
3	760	2	WQ	525	4	1398	1334	8.9	20
4	760	4	FC	530	6	971	911	22.6	51
5	790	1	AC	525	6	1437	1370	9.6	18
6	790	1	WQ	530	4	1397	1332	8.1	16
7	790	2	FC	520	2	1026	948	18.3	42
8	790	4	WQ	535	2	1306	1249	13.7	26
9	810	1	FC	530	4	1206	1109	12.1	22
10	810	2	AC	525	2	1219	1150	10.3	19
11	810	2	WQ	535	4	1311	1235	7.4	11
12	810	4	WQ	520	6	1357	1272	8.6	13
13	840	1	FC	520	2	1103	1016	16.1	34
14	840	2	AC	530	6	1323	1240	8.2	14
15	840	4	AC	535	4	1302	1224	9.2	14
16	840	4	WQ	525	2	1190	1101	8.8	18
17	870	1	WQ	530	2	1286	1198	9.4	16
18	870	1	WQ	535	2	1286	1199	9.7	14
19	870	2	AC	525	4	1328	1255	8.7	13
20	870	2	FC	535	6	1169	1073	12.4	20
21	870	4	AC	520	4	1336	1265	8.4	12
22	900	1	FC	525	4	1189	1105	10.1	16
23	900	2	WQ	530	2	1227	1137	8.8	13
24	900	2	AC	535	4	1295	1208	7.1	11
25	900	4	AC	520	6	1344	1264	6.3	9

while those corresponding to A and Z are different, that is, there are two distinct optimal factor level combinations for different indices. Considering the strength and plasticity of the material comprehensively, the optimal factor level combination should be $A_2B_1C_{1/3}D_{2/3}E_{1/2}$.

3.2 Effect of factors on mechanical properties

According to the analysis of the orthogonal experiment, factor C is found to be the most significant factor, while the influence order of the other four factors on the indexes is A>E>D>B. Therefore, samples with different levels of factors C and A were selected for microstructure observation according to the influence degree of the factors on the mechanical properties.

Fig. 2 shows the microstructure of as-forged TB18 alloy, consisting of a β matrix and equiaxed α phases. Fig. 3 shows the microstructures after heat treatment at different levels of factor C. According to Table 3, the order of tensile strength and yield strength under different solution cooling methods is AC>WQ>FC. Typically, a higher cooling rate results in a greater degree of instantaneous supercooling, thereby increasing the nucleation rate of the α phase[22]. At a solution temperature of 790 °C, AC exhibits a relatively slow rate with a moderate supercooling degree, which provides sufficient nucleation driving force to promote homogeneous nucleation of the α phase. This allows for the retention of a portion of the α_p phase while facilitating the precipitation of fine lamellar α_s phase, yielding a significant strengthening effect. By contrast, WQ induces excessive supercooling, which suppresses the nucleation of the α phase and hinders the precipitation of secondary phases, thus exhibiting a weaker strengthening effect compared to AC. In comparison, FC proceeds at a slow rate with minimal supercooling. During the slow cooling process, the precipitated secondary phases absorb other solute elements in the vicinity of nucleation sites, undergoing coarsening and growth. This microstructural evolution ultimately leads to lower strength.

However, the aging time for the alloy solution treated with WQ (Fig. 3c–3d) is 2 h shorter than that solution treated with AC (Fig. 3a – 3b), resulting in weaker aging strengthening effects and lower strength for WQ compared to AC. The differences in strength and plasticity are primarily related to the coarsening of α_s phase. Comparing the Fig. 3b, 3d, and 3f, significant coarsening can be found for α_s phase, which reduces dislocation slip resistance and weakens precipitation

Table 4 Analysis of orthogonal test results

Evaluation index	Mean value and range	A	B	C	D	E	Blank column
R_m/MPa	$\bar{k}_1$	1280.5	1295.2	1333.7	1227.3	1226.8	1196.3
	$\bar{k}_2$	1291.5	1255.1	1306.4	1293.5	1306.9	1301.8
	$\bar{k}_3$	1273.0	1258.0	1110.7	1235.0	1279.4	1322.1
	$\bar{k}_4$	1229.5	-	-	1289.1	-	-
	$\bar{k}_5$	1281.0	-	-	-	-	-
	$\bar{k}_6$	1263.8	-	-	-	-	-
	R	62.0	40.1	223.0	66.2	80.1	125.8
$R_{p0.2}$/MPa	$\bar{k}_1$	1220.0	1218.2	1261.1	1183.2	1148.0	1148.0
	$\bar{k}_2$	1224.8	1175.6	1228.6	1219.2	1229.7	1204.4
	$\bar{k}_3$	1191.5	1183.7	1027.0	1154.5	1204.4	1120.4
	$\bar{k}_4$	1145.3	-	-	1212.7	-	-
	$\bar{k}_5$	1198.0	-	-	-	-	-
	$\bar{k}_6$	1178.5	-	-	-	-	-
	R	79.5	42.6	234.1	64.7	81.7	84.0
A/%	$\bar{k}_1$	12.2	10.3	8.5	10.9	11.4	12.1
	$\bar{k}_2$	12.4	10.0	9.3	9.4	8.9	9.9
	$\bar{k}_3$	9.6	11.1	15.3	11.5	11.1	9.0
	$\bar{k}_4$	10.6	-	-	9.9	-	-
	$\bar{k}_5$	9.7	-	-	-	-	-
	$\bar{k}_6$	8.1	-	-	-	-	-
	R	4.3	1.1	6.8	2.1	2.5	3.1
Z/%	$\bar{k}_1$	28.3	19.8	15.2	21.7	22.4	24.7
	$\bar{k}_2$	25.5	18.1	16.3	17.3	15.0	17.5
	$\bar{k}_3$	16.3	20.4	30.8	22.0	21.0	15.3
	$\bar{k}_4$	20.0	-	-	16.9	-	-
	$\bar{k}_5$	18.8	-	-	-	-	-
	$\bar{k}_6$	12.3	-	-	-	-	-
	R	16.0	2.3	15.6	5.1	7.4	9.4

strengthening. Coarsened α_s phase also tortuously extends crack propagation paths, increasing crack resistance and enhancing alloy ductility and fracture toughness. Therefore, as α_s coarsens, the strength decreases while plasticity increases[23].

To analyze the influence of different solution temperatures (A) on the microstructure of the alloy, the optical microstructures of TB18 alloy after solution treatment at 790 and 870 °C were characterized. As shown in Fig.4a, when the solution treatment temperature is lower than the phase transition temperature and followed by aging treatment, since the solution temperature falls within the temperature rarge of the dual-phase region, the alloy structure is composed of fine β grains and a small amount of equiaxed α_p phase (Fig.4a and Fig.5a), and the recrystallized β grains have fine corners with discontinuous grain boundaries. After aging, the α_s phase precipitates in the form of fine lamellae (Fig. 5b). With the increase in solution temperature, the volume fraction of α_p decreases, and the concentration of solute atoms in the metastable β matrix increases. When the solution treatment temperature is higher than the β-phase transition temperature, and solution treatment is followed by aging treatment, as shown in Fig. 4b, obvious grain boundaries are formed, and the recrystallized β grains are coarsened. However, the increase in solution temperature improves the solubility of alloying elements in the β phase, making the supersaturated solid solution more stable. After aging, the lamellar α_s phase precipitated from the metastable β matrix is formed synchronously inside the grains and at the grain boundaries, and it is uniformly distributed in the β matrix. The lamellar α phases usually maintain a specific crystallographic orientation relationship with the β matrix, since the atomic arrangements of α and β phases are similar and can match well during aging. After α phase nucleation, the growth rate in the thickness direction is slower than that in the vertical direction, thus forming lamellar α phase[24]. Although the β grains are coarsened after solution treatment at 870 ° C, their yield strength (1255 MPa) does not decrease excessively due to grain coarsening, being only 115 MPa lower than that of the alloy after solution treatment at 790 °C. In TB18 alloy, there are significant differences in the formation mechanism, morphology, and strengthening effect between the α_p phase and the α_s phase. The α_p phase is formed during hot working in

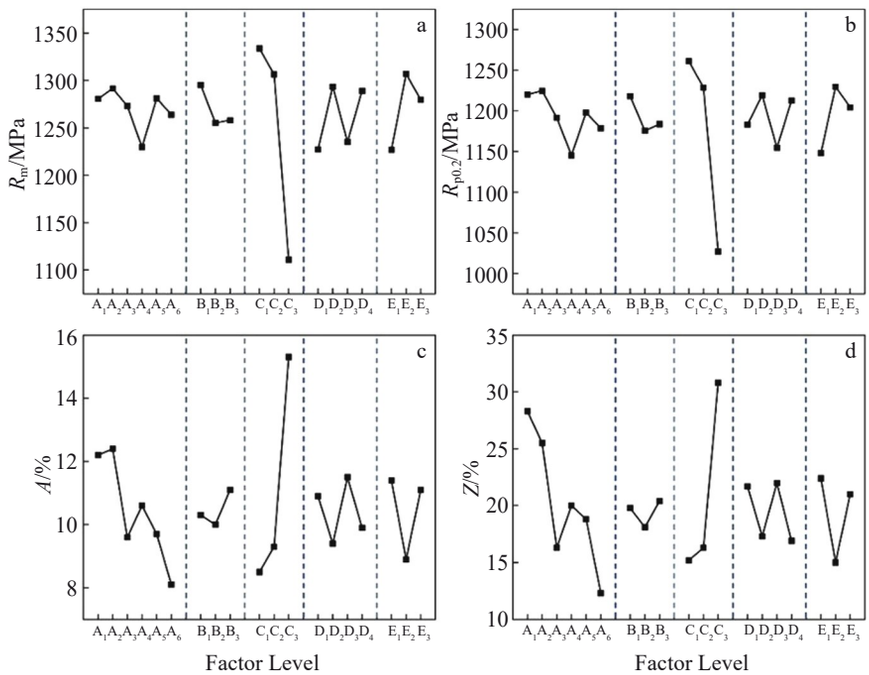

Fig.1 Relationships between factor level and different evaluation indices: (a) R_m; (b) $R_{p0.2}$; (c) A; (d) Z

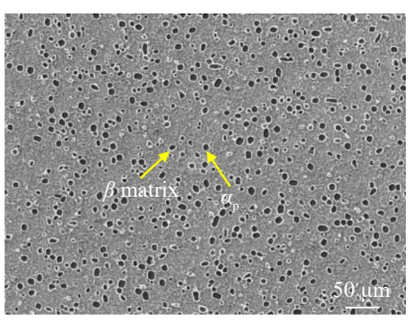

Fig.2 Microstructure of as-forged TB18 alloy

the α+β dual-phase region or solution treatment at a relatively low temperature, presenting an equiaxed shape and mainly distributed at the boundaries or inside the β grains. Its existence can improve strength through dispersion strengthening and inhibiting the coarsening of β grains, while retaining a certain degree of plasticity. The α_s phase, on the other hand, is formed during the aging process, precipitated from the supersaturated β solid solution with a lamellar or acicular morphology and distributed within the β grains. It enhances strength through precipitation strengthening, and its strengthening effect is closely related to its size and distribution. More significant strengthening effects are exhibited by fine spherical or thin lamellar α_s phases, while the strengthening effect is weakened after coarsening. Under the solution treatment condition of 870 °C, since the temperature is higher than the β-phase transition temperature, the α_p phase completely dissolves, resulting in the disappearance of its dispersion strengthening effect. At the same time, the β grains are coarsened, the number of grain boundaries is reduced, and the grain boundary strengthening effect is weakened. However, due to the increase in solution temperature, the supersaturation degree of the β phase increases, leading to more uniform precipitation of the α_s phase during aging. Therefore, although there is a slight coarsening compared to the α_s phase after solution treatment at 790 °C due to the higher temperature, the continuous distribution of the lamellar α_s phase can still provide strong precipitation strengthening, which partially offsets the adverse effects of the dissolution of α_p phase and the coarsening of grains. As a result, the strength decreases slightly and remains at a high level.

According to Table 3, the yield strength and tensile strength decrease with the increase in solution temperature. This may be related to the dissolution of α_p phase and coarsening of α_s phase during solution treatment. The volume fraction of α_p phase decreases with the increase in solution temperature. The hexagonal close-packed α_p phase has higher deformation resistance than the body-centered cubic β phase. Thus, the strength decreases with the increase in temperature. When the alloy is solution-treated at a relatively high temperature, the phase transformation driving force is small, and the nucleation driving force of α_s phase is insufficient, which affects the nucleation of α_s phase. Besides, the coarsening of α_s phase is a thermally activated process, and its coarsening rate depends on the diffusion of solute atoms[25]. The diffusion rate gets higher as temperature increases, resulting in easy formation of the large-sized α phase and leading to a decrease in plasticity. In summary, the optimal heat treatment parameters for TB18 alloy are as follows: solution temperature of 790 °C, solution holding time of 1 h, solution cooling mode of AC, aging temperature of 525–530 °C, and aging time of 2–4 h.

3.3 Relationship between impact toughness and microstructure at different solution temperatures

As discussed in the previous section, the heat treatment

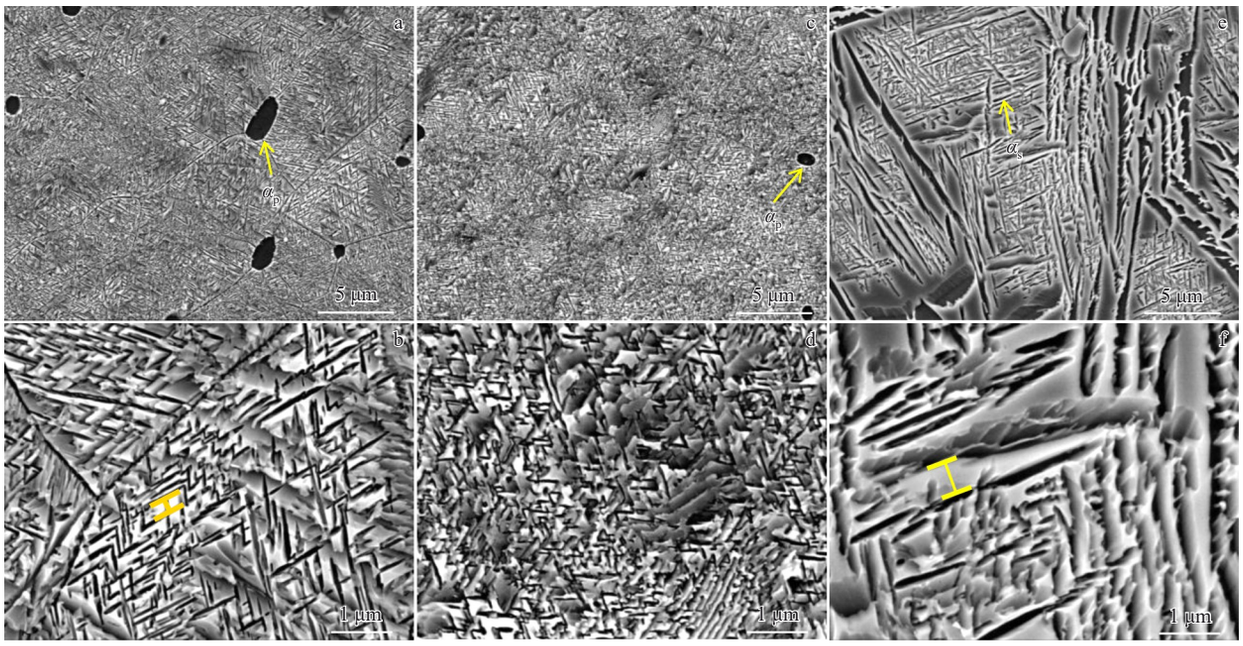

Fig.3 Microstructures of TB18 alloy after different heat treatments: (a–b) 790 °C/1 h, AC+525 °C/6 h, AC; (c–d) 790 °C/1 h, WQ+530 °C/4 h, AC; (e–f) 790 °C/2 h, FC+520 °C/2 h, AC

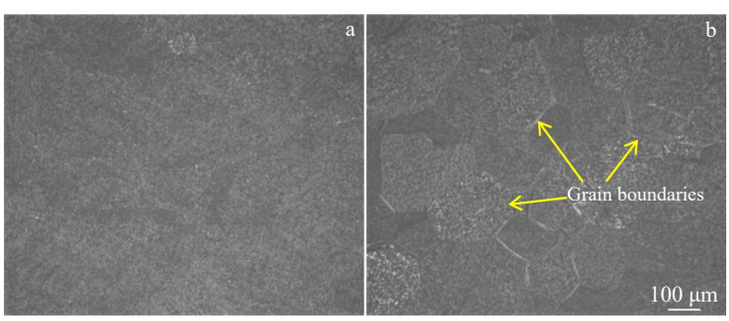

Fig.4 OM images of TB18 alloy after different heat treatments: (a) 790 °C/1 h, AC+525 °C/6 h, AC; (b) 870 °C/2 h, AC+525 °C/4 h, AC

process parameters for the optimal strength-ductility combination are the solution temperature of 790 °C, solution holding time of 1 h, solution cooling mode of AC, aging temperature of 525 – 530 °C, and aging time of 2 – 4 h. Considering the influence order of various factors on strength-ductility during solution and aging treatment, the parameters of solution holding time of 1 h, solution cooling mode of AC, aging temperature of 525 °C, and aging time of 4 h were selected to further investigate the effects of solution temperature in the range of 790 – 870 °C on the impact toughness and micro-fracture characteristics of the alloy.

Table 5 shows the oscilloscopic impact test data at different solution temperatures. With the increase in solution temperature, the absorbed energy increases from 15 J to 24 J, indicating that the impact toughness of the alloy is enhanced with the increase in solution temperature. The initiation energy is 4 J at 790 and 870 °C and 3 J at 810 and 840 °C, suggesting that the solution temperature has a weak effect on the difficult degree of crack initiation. However, the propagation energy increases from 11 J to 20 J with the increase in solution temperature, showing an increase rate of 81.8%, which is the main contributor to the increase in absorbed energy. This indicates that the energy dissipation during crack propagation is the core mechanism, by which the solution temperature regulates toughness.

Fig. 6 shows the overall fracture morphologies of the TB18 alloy solution treated at different temperatures. The marked areas 1, 2, and 3 are the three characteristic regions of the fracture, which are the shear lip zone, the fibrous zone, and the radial zone, respectively. It can be clearly seen that the area fraction of each region in the fractures at different solution temperatures is different. Statistical analysis of the impact fracture surfaces at different solution temperatures in Fig. 6 was performed using Image-Pro Plus image analysis software. It is found that as the solution temperature increases from 790 °C to 870 °C, the area fraction of the shear lip region increases from 5% to 12%, and the area fraction of the fibrous region increases from 30% to 45%. The impact energy is higher when the areas of the shear lip zone and fibrous zone are larger and the radial zone area is smaller. The radial zone

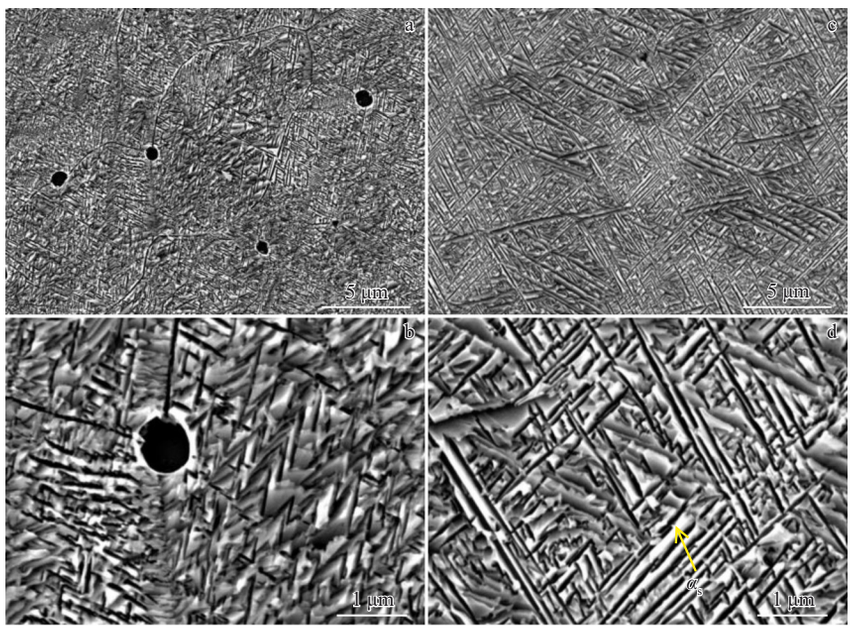

Fig.5 Microstructures of TB18 alloy solution treated at different temperatures: (a–b) 790 °C/1 h, AC+525 °C/6 h, AC; (c–d) 870 °C/2 h, AC+525 °C/4 h, AC

Table 5 Results of oscilloscopic impact test for TB18 alloy solution treated at different temperatures

Solution temperature/°C	Absorbed energy, W_t/J	Initiation energy, W_i/J	Propagation energy, W_p/J
790	15	11	4
810	20	17	3
840	21	18	3
870	24	20	4

is a typical feature of brittle fracture, and its area fraction decreases from 65% (at 790 °C) to 43% (at 870 °C), indicating that high-temperature solution treatment significantly decreases the proportion of brittle fracture. Combined with the observation of the microstructure, due to the uniform distribution of the lamellar α_s phase after solution treatment at 870 °C, the crack propagation path changes from radial straight propagation to tortuous propagation, which inhibits the formation of the radial zone.

Changes in the main crack direction are usually accompanied by the generation of secondary cracks. Fig. 7 shows the morphologies of secondary cracks observed on the fracture surfaces of the TB18 alloy solution treated at different

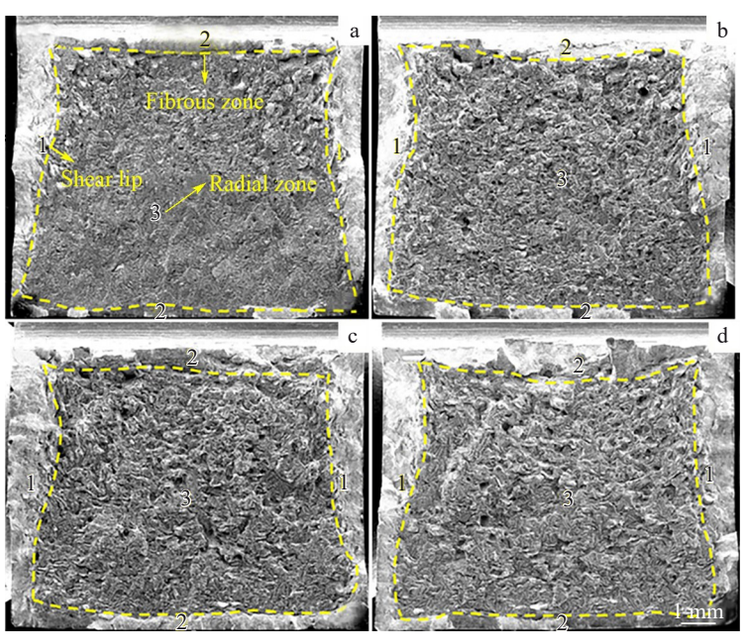

Fig.6 Impact fracture morphologies of TB18 alloy solution treated at different temperatures: (a) 790 °C; (b) 810 °C; (c) 840 °C; (d) 870 °C

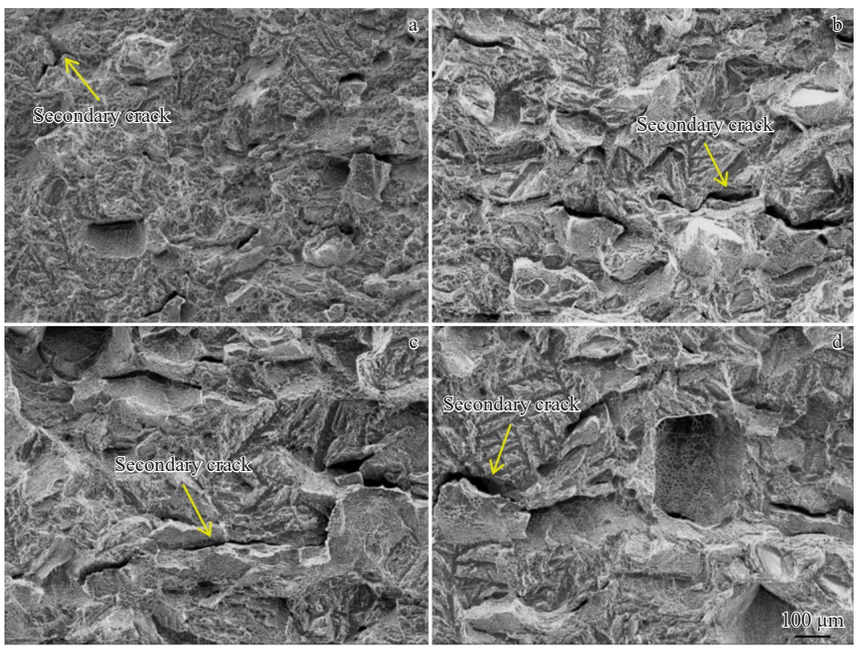

Fig.7 Secondary cracks on fracture surface of TB18 alloy solution treated at different temperatures: (a) 790 °C; (b) 810 °C; (c) 840 °C; (d) 870 °C

temperatures, as indicated by the yellow arrows. It can be seen that with the increase in solution temperature, the length of secondary cracks in the impact fractures gradually increases. After solution treatment at 870 °C, the α_s phase precipitated during aging is uniformly distributed in a lamellar form within the coarse β grains. There is a significant difference in mechanical properties at the interface between the α_s phase and the β phase. Under impact loading, the lamellar α_s phase, acting as a hard phase, causes stress concentration at its interface with the β phase. When the local stress exceeds the critical fracture strength of the material, secondary cracks will be initiated between the α_s phase layers near the main crack or in the β phase matrix to release the concentrated stress. In the alloy solution treated at 790 °C, the fine β grains restrict the extension of cracks, and the stress concentration cannot accumulate enough energy required for the nucleation of secondary cracks, resulting in short and few secondary cracks. The higher the solution temperature, the more sufficient the space provided by the coarse β grains for the growth of secondary cracks, enabling the secondary cracks to extend along the continuous distribution direction of the lamellar α_s phase and further consume the impact energy. In addition, in samples with low impact energy, a large number of quasi-cleavage planes were observed, as shown in Fig. 8a. With the increase in solution temperature, the number of dimples in the fracture morphology increases. As shown in Fig. 8, after solution treatment at 790 °C, a small amount of equiaxed α_p phase is retained in the structure. As a hard phase, the interface between the α_p phase and the β phase tends to become a nucleation site for micro-voids. Due to the small size and dispersed distribution of the α_p phase, the nucleation of micro-voids is dense but the growth space is restricted, thus forming shallow and dense dimples. Under stress, the micro-voids grow rapidly and coalesce, with insufficient plastic deformation and little energy consumption. After solution treatment at 870 °C, the α_p phase completely dissolves, and the lamellar α_s phase is uniformly distributed in the coarse β grains. At this time, micro-voids are mainly nucleated at the interface between the α_s phase and the β phase, and the coarse β grains provide sufficient space for the growth of micro-voids. On the one hand, the continuity of the lamellar α_s phase makes the nucleation of micro-voids more uniform; on the other hand, the β phase matrix can undergo large plastic deformation under impact loading, which promotes the ductile tearing of the matrix during the growth of micro-voids. The growth of micro-voids needs to overcome the plastic deformation resistance of the β phase. Under impact loading, the lamellar α_s phase can coordinate the plastic deformation of the β phase through its own slip, enabling the material to accumulate greater plastic deformation before fracture, eventually forming deeper dimples and enhancing the toughness of the material.

As shown in Fig. 9, the crack propagation paths are observed in fractures with obvious tortuous changes in the paths (Fig. 9a–9c). At a solution temperature of 790 °C, since the alloy is in the dual-phase region, the microstructure contains a small amount of α_p and α_s. During impact, cracks can directly propagate through the relatively soft α_p phase, as shown in Fig. 10a. In contrast, lamellar α_s phase is harder, and the coarser the lamellar α_s, the more difficult the crack penetration. Therefore, cracks bypass the α_s phase, leading to more tortuous propagation paths, consuming more energy, and thus improving the toughness of the alloy. The kinking deformation of lamellar α phase is circled by yellow dashed lines in Fig. 11. Besides, cracks are usually accompanied by the formation of holes, as shown in Fig. 10b–10d.

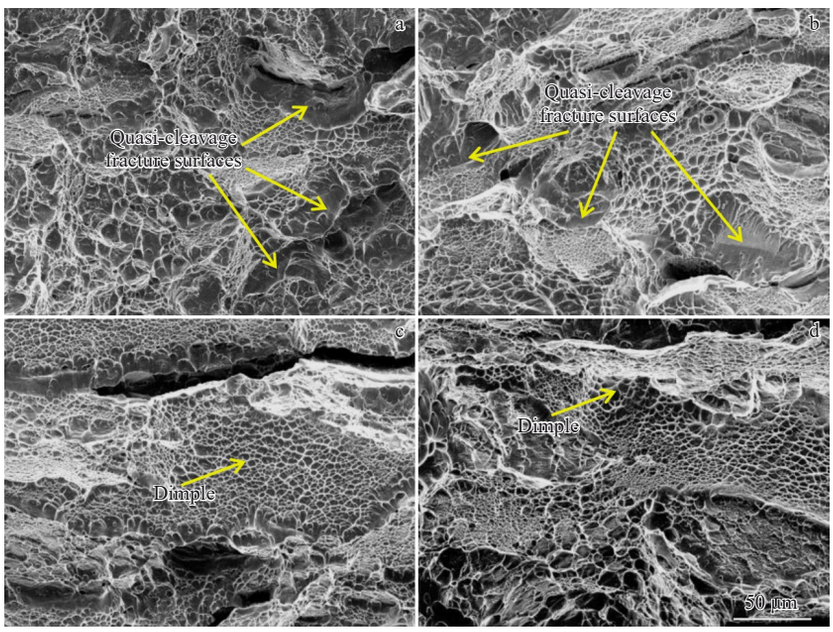

Fig.8 Impact fracture morphologies of TB18 alloy solution treated at different temperatures: (a) 790 °C; (b) 810 °C; (c) 840 °C; (d) 870 °C

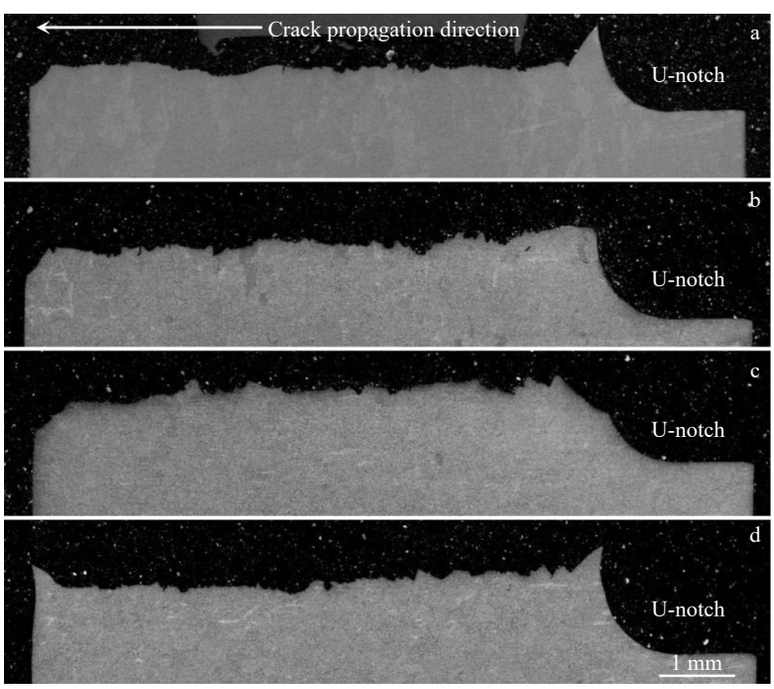

Fig.9 Crack propagation paths of impact fracture of TB18 alloy solution treated at different temperatures: (a) 790 °C; (b) 810 °C; (c) 840 °C; (d) 870 °C

3.4 Relationship between impact toughness and microstructure at different aging temperatures

To investigate the effect of precipitation behavior of α_s phase on impact toughness, the TB18 alloy solution treated at 870 ° C/1 h in the single-phase region was then aged at different temperatures. Oscilloscopic impact tests were conducted on the samples, and the results of absorbed energy, crack initiation energy, and crack propagation energy are shown in Table 6. With the increase in aging temperature, the propagation energy decreases significantly, making the initiation energy dominate. The impact absorbed energy also decreases significantly first and then slightly increases with the increase in aging temperature, as shown in Fig.12.

The microstructures of the samples aged at different temperatures were observed via SEM. At an aging temperature of 450 °C, the precipitation of secondary phase is less obvious, with α_s phases mainly precipitating along grain boundaries and arranging in parallel. As the aging temperature increases to 525 °C, a large number of α_s phases are uniformly

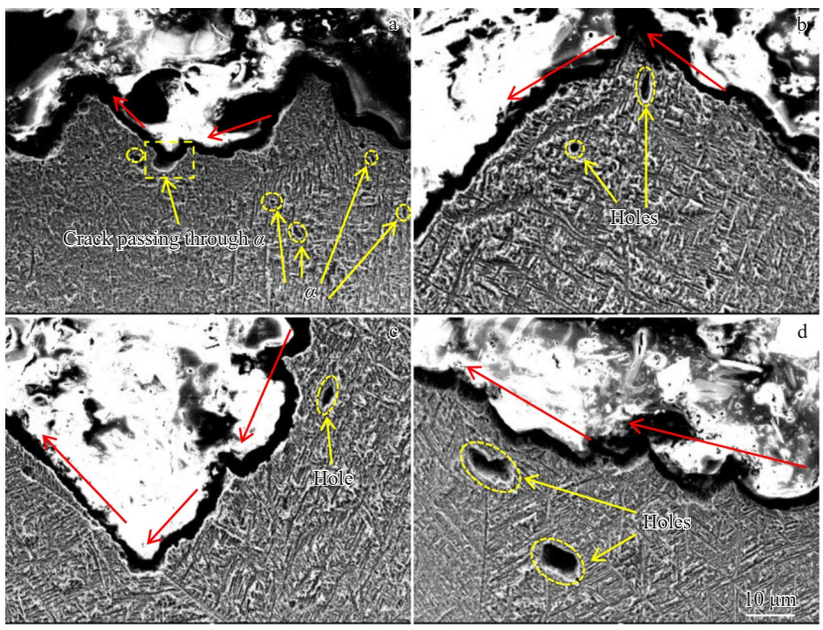

Fig.10 Cracks passing through α phase and formation of holes in TB18 alloy solution treated at different temperatures: (a) 790 °C; (b) 810 °C; (c) 840 °C; (d) 870 °C

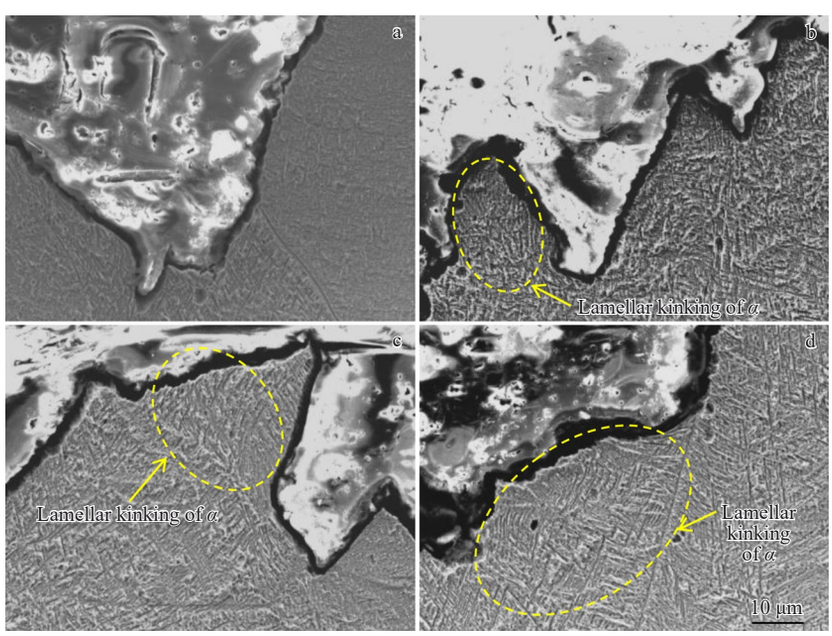

Fig.11 Plastic deformation around cracks in TB18 alloy solution treated at different temperatures: (a) 790 °C; (b) 810 °C; (c) 840 °C; (d) 870 °C

Table 6 Results of oscilloscopic impact test for TB18 alloy solution treated at 870 °C/1 h followed by aging at different temperatures

Aging temperature/°C	Absorbed energy, W_t/J	Initiation energy, W_i/J	Propagation energy, W_p/J
450	60.3	26.9	33.4
490	21.5	17.8	3.7
525	22.1	20.3	1.8
570	34.3	25.7	8.6

and dispersedly precipitated and interweave with each other. When the aging temperature further rises, the thickness of the precipitated lamellae α_s increases, with the orientations becoming more ordered, forming secondary α_s clusters with roughly the same internal orientation within β grains, as shown in Fig.13.

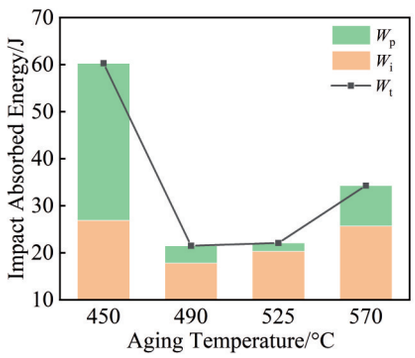

Fig.12 Variation in impact absorbed energy of TB18 alloy solution treated at 870 °C/1 h followed by aging at different temperatures

Observation of the fracture morphology and crack propagation path of the samples aged at different temperatures reveals that, compared to the solution-treated state alloy, the impact crack initiation and propagation path is relatively straight in the aged alloy. The morphologies of the fracture surfaces in the samples aged at 490 and 525 °C are the smoothest, with the smallest shear lip area, indicating rapid crack propagation, while the solution-treated samples exhibit the largest number and size of dimples. In contrast, the aged samples have shallower dimples and cleavage planes, and they show characteristics of intergranular fracture, suggesting lower energy consumption during crack propagation (Fig.14). The optimal heat treatment process for comprehensive strength-plasticity-toughness of TB18 alloy is 870 °C/1 h,

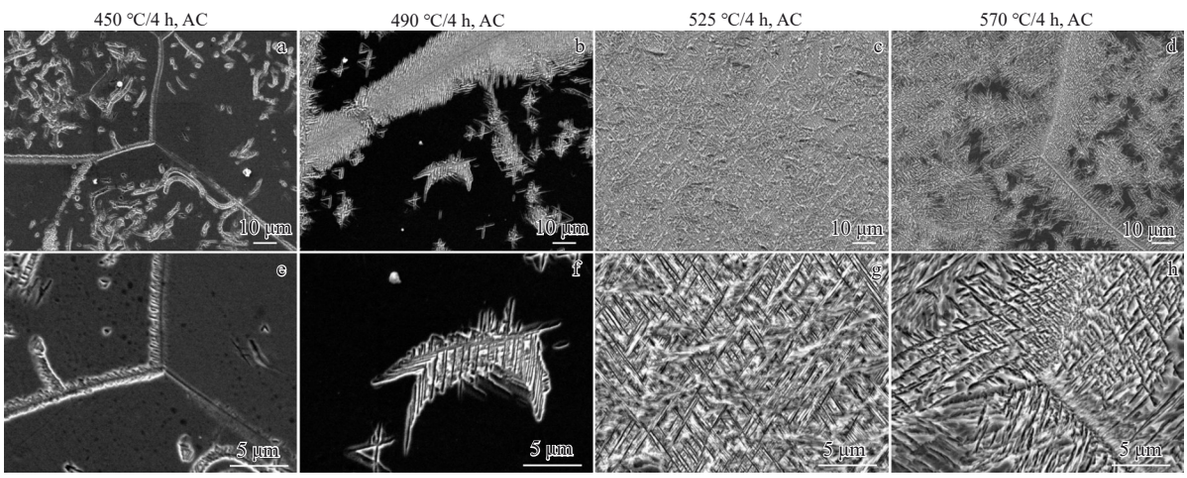

Fig.13 Microstructures of TB18 alloy aged at different temperatures: (a, c) 450 °C; (b, d) 490 °C; (c, e) 525 °C; (d, f) 570 °C

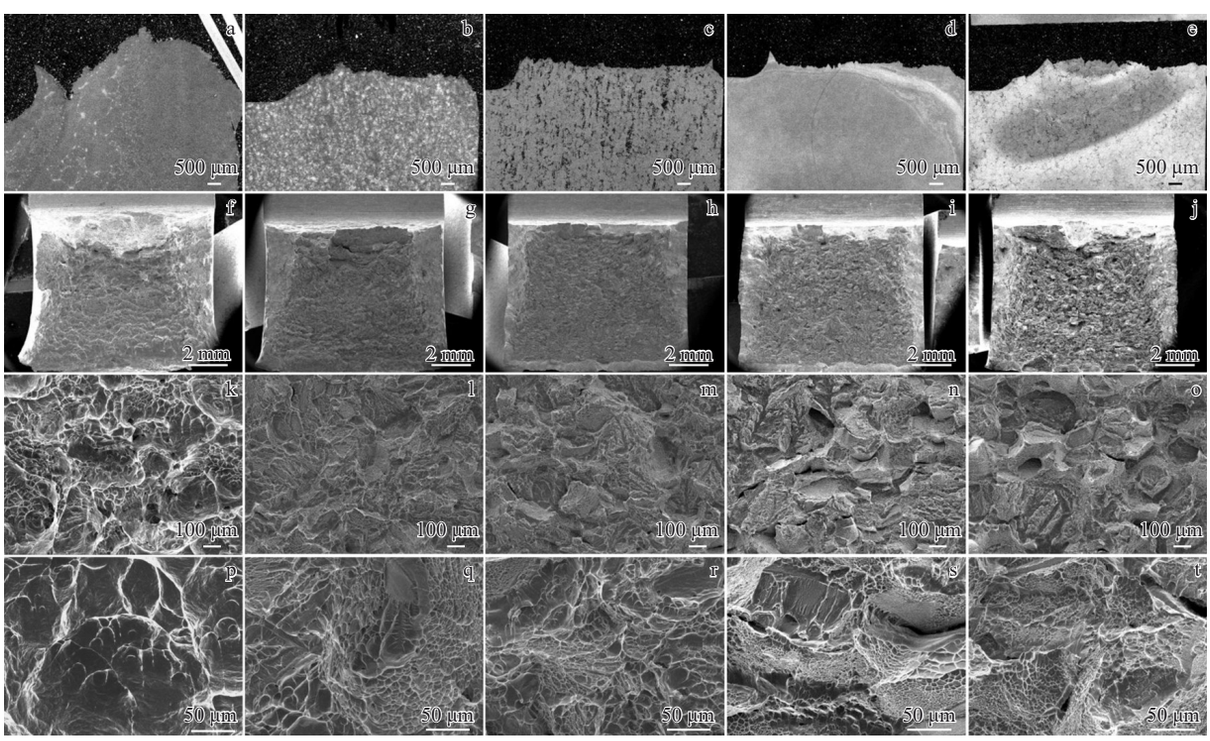

Fig.14 Impact fracture morphologies and crack propagation paths of TB18 alloy aged at different temperatures: (a, f, k, p) solution state; (b, g, l, q) 450 °C; (c, h, m, r) 490 °C; (d, i, n, s) 525 °C; (e, j, o, t) 570 °C

AC+525 °C/4 h, AC.

4 Conclusions

1) The influence order on the R_m, $R_{p0.2}$, A, and Z of TB18 alloy is: solution cooling method>solution temperature>aging time>aging temperature>solution holding time. The optimal heat treatment parameters for comprehensive strength-ductility are as follows: solution temperature of 790 ° C, solution holding time of 1 h, solution cooling method of AC, aging temperature of 525–530 °C, and aging time of 2–4 h.

2) The tensile properties of TB18 alloy under different heat treatments largely depend on the content, size, and morphology of the α_s phase. Therefore, the α_s phase is a critical factor affecting the strength and plasticity of TB18 alloy.

3) The area fraction of the shear lip zone, the fibrous zone, and the radial zone in the fracture morphology of TB18 alloy directly reflects the toughness of the alloy. Larger areas of the shear lip and fibrous zone with a smaller radial zone indicate better toughness. Longer secondary crack length and deeper dimples also signify better toughness. Alloys with better toughness exhibit tortuous crack propagation paths and intense plastic deformation around the crack propagation path.

4) The influence of solution temperature on impact toughness is significantly weaker than that of the aging process for TB18 alloy, providing restricted guidance for regulating and analyzing its impact toughness. In contrast, the morphological distribution of the secondary phase during aging has a more significant effect on performance. The optimal heat treatment process for comprehensive strength-plasticity-toughness of TB18 alloy is 870 ° C/1 h, AC+525 °C/4 h, AC.

References

1 Wang T, Feng Y, Liu X H *et al*. *Materials*[J], 2022, 15(12): 4068

2 Liu Z M, Xin S W, Zhao Y Q. *Metals*[J], 2023, 13(12): 1975

3 Liu Xianghong, Zhao Ning, Wang Tao *et al*. *Rare Metal Materials and Engineering*[J], 2024, 53(11): 3101 (in Chinese)

4 Wang Linzeng, Yu Jun, Lin Xin *et al*. *Foundry Technology*[J], 2025, 46(2): 144 (in Chinese)

5 Popov A A, Petrova A O, Narygina I V *et al*. *Physics of Metals and Metallography*[J], 2024, 125(12): 1457

6 Zhang J S, Gao E D, Wang Z B *et al*. *Journal of Materials Engineering and Performance*[J], 2025, 34: 19122

7 Chong Y, Gholizadeh R, Guo B Q *et al*. *Acta Materialia*[J], 2023, 257: 119165

8 Liu L L, Huang M D, Geng D H *et al*. *Materials Science and Engineering A*[J], 2024, 891: 145970

9 Naydenkin E V, Mishin I P, Zabudchenko O V *et al*. *Journal of Alloys and Compounds*[J], 2023, 935: 167973

10 Wang Hua, Cao Le, Wu Tiandong. *Foundry Technology*[J], 2025, 46(1): 87 (in Chinese)

11 Zhang L H, Rittel D, Osovski S. *Materials Science and Engineering A*[J], 2018, 729: 94

12 Wang K G, Wu D, Wang D *et al*. *Materials Science and Engineering A*[J], 2022, 829: 142151

13 Xu Y F, Liu H Q, Zhang S *et al*. *Journal of Materials Research and Technology*[J], 2022, 18: 2870

14 Ji Xiaoyu, Xu Jianwei, Zhang Yu *et al*. *Rare Metal Materials and Engineering*[J], 2025, 54(3): 665 (in Chinese)

15 Yu G X, Zhao D X, Li K *et al*. *Materials Science and Engineering A*[J], 2022, 858: 144180

16 Li X, Wang X N, Liu K *et al*. *Journal of Materials Research and Technology*[J], 2022, 21: 4860

17 Yano R, Tanaka M, Yamasaki S *et al*. *Materials Transactions*[J], 2024, 65(10): 1260

18 Xiang W, Xiang Y, Zhang F *et al*. *Materials Science and Engineering A*[J], 2024, 893: 146125

19 Li Bo, Qin Fengying, Lin Yuan *et al*. *Transactions of Materials and Heat Treatment*[J], 2025, 46(2): 122 (in Chinese)

20 Fu Q, Xiang W, Yuan W H *et al*. *Journal of Materials Science*[J], 2024, 59: 6986

21 Jia Y D, Cao S, Ma Y J *et al*. *Acta Metallurgica Sinica (English Letters)*[J], 2023, 36: 1844

22 Gupta A, Khatirkar R K, Kumar A *et al*. *Journal of Materials Research*[J], 2018, 33(8): 946

23 Yuan C, Liu D, Xu X C *et al*. *Journal of Materials Research and Technology*[J], 2024, 33: 39

24 Zheng H J, Fan X G, Zeng X *et al*. *Chinese Journal of Aeronautics*[J], 2019, 32(5): 1305

25 Lei L, Zhao Q Y, Wu C *et al*. *Journal of Materials Science & Technology*[J], 2022, 99: 101

TB18钛合金固溶时效工艺正交优化及韧性调控机制

高慧贤[1,2]，李　科[2]，邵　珊[2]，杨浩雪[1]，李芹芹[1,2]，赵燕茹[2]，罗文忠[1,2]，
冯　勇[1,2]，雷　强[1,2]，刘向宏[1,2]
(1. 西北工业大学 材料学院，陕西 西安 710072)
(2. 西部超导材料科技股份有限公司，陕西 西安 710018)

摘　要：为探究固溶时效工艺参数对TB18钛合金微观组织与力学性能的影响规律，基于混合正交试验因素水平试验设计开展工艺优化研究。结果表明，结合极差分析确定工艺参数影响显著性顺序为：固溶冷却方式>固溶温度>时效时间>时效温度>固溶时间。综合强塑性匹配与工程应用需求，选定固溶时间1 h、固溶冷却方式空冷（AC）、时效温度525 ℃、时效时间4 h为基准参数，进一步研究790~870 ℃固溶温度区间对合金冲击韧性及微观断口特征的影响。结果显示，剪切唇和纤维区面积越大，放射区面积越小，合金韧性越优；随固溶温度升高，断口二次裂纹长度增加，韧窝数量增加，韧性增强。基于强塑韧性协同优化，确定TB18合金最优的热处理工艺为870 ℃/1 h, AC+525 ℃/4 h, AC。

关键词：TB18钛合金；固溶时效；正交试验；韧性；微观组织

作者简介：高慧贤，女，1981年生，硕士，高级工程师，西部超导材料科技股份有限公司，陕西 西安 710018，E-mail：gaohuixian@c-wst.com